Colloids and Surfaces B: Biointerfaces 211 (2022) 112283

Contents lists available at ScienceDirect

Colloids and Surfaces B: Biointerfaces

journal homepage: www.elsevier.com/locate/colsurfb

# Self-adhering implantable device of titanium: Enhanced soft-tissue adhesion by sandblast pretreatment

Atsushi Yabe [a,b,c], Masahiro Okada [a,*], Emilio Satoshi Hara [a], Yasuhiro Torii [b,c], Takuya Matsumoto [a,*]

[a] Department of Biomaterials, Graduate School of Medicine, Dentistry and Pharmaceutical Sciences Okayama University, 2-5-1 Shikata-cho, Kita-ku, Okayama 700-8558, Japan

[b] Department of Comprehensive Dentistry, Graduate School of Medicine, Dentistry and Pharmaceutical Sciences, Okayama University, 2-5-1 Shikata-cho, Kita-ku, Okayama 700-8558, Japan

[c] Comprehensive Dental Clinic, Okayama University Hospital, 2-5-1 Shikata-cho, Kita-ku, Okayama 700-8558, Japan

ARTICLE INFO

*Keywords:*
Titanium
Soft tissue adhesion
Acid treatment
Sandblasting

ABSTRACT

Self-adhering implantable devices, which can be immobilized inside the bodies without suturing nor organic glues, made of metallic biomaterials would be optimal devices for preventing device-related complications such as device migration after implantation. We reported previously that acid-treated commercially-pure titanium (CpTi) adhered directly and immediately on hydrous non-keratinized soft tissues. Herein, we investigated the influence of sandblasting as pretreatment for acid-treated CpTi to increase its soft tissue adhesiveness. First, the effects of sandblasting conditions (*i.e.*, pressure, distance and time) were investigated in terms of the sandblasted surface area and the degree of deformation (*i.e.*, internal stress formation) of CpTi films. The effect of the sandblasting on the immediate soft tissue adhesion of acid-treated CpTi was investigated using an *ex vivo* shear adhesion test with mouse dermal tissues. The optimal sandblasting pretreatment remarkably improved the soft tissue adhesion strength of acid-treated CpTi (102 ± 19 kPa) compared with the non-sandblasted counterparts (41 ± 2 kPa). Finally, the CpTi adhesive was applied for immobilizing a near field communication (NFC) device *in vivo*, and was shown to have strong immediate adhesion to muscle fascia.

## 1. Introduction

In the recent advancement of the Internet of Things (IoT) society, implantable devices such as biochips and biosensors have been paid great attention [1–3]. As a biochip, injectable radio frequency identification (RFID) tag [4] or near-field communication (NFC) chip have now widely helped to manage livestock, domesticated or laboratory animals and products in the food supply chain. Biosensors have been developed to be used not only as a monitoring system of the biorhythms [3], but also as a drug release system for the treatment of cancers or endocrine diseases, including diabetes [5]. In the near future, these implantable devices are expected to be important tools for human electronic identification, internal body monitoring and also prevention and/or treatment of diseases. Nevertheless, the migration (*i.e.*, intra-body mobility) of implantable devices, including the current injectable RFID tag [6,7], is still one of the major problems hindering their further application.

Surgical sutures are currently used for immobilization of body-implanted electrical stimulation therapy devices, such as artificial pacemakers [8], deep brain stimulation (DBS) [9] and spinal cord stimulation (SCS) [10,11] devices, and the common hardware-related complications also include the migration of electrode leads [8–11] and pulse generators [12–14]. Moreover, the suturing technique is time-consuming and highly dependent on the physician's skills, and hence often result in secondary tissue damage, microbial infection, fluid or air leakage, and poor cosmetic outcome [15]. Additionally, the suturing technique is sometimes inadequate due to the patients' conditions, such as insufficient or fragile tissues [16], and due to the type of devices (*e.g.*, small injectable devices cannot be immobilized by suturing). An appealing option to sutures is the use of tissue adhesives such as cyanoacrylate [17], gelatin-resorcinol-formaldehyde/glutaraldehyde (GRFG) [18] and fibrin [19] glues. However, cyanoacrylate and GRFG show relatively toxic reactions, and fibrin lacks adhesion strength [20]. Besides, those glues need time-consuming setting reactions. More recently, researchers have developed unique adhesives with higher

* Corresponding authors.
*E-mail addresses:* m_okada@cc.okayama-u.ac.jp (M. Okada), tmatsu@md.okayama-u.ac.jp (T. Matsumoto).

https://doi.org/10.1016/j.colsurfb.2021.112283
Received 28 October 2021; Received in revised form 6 December 2021; Accepted 8 December 2021
Available online 10 December 2021

**Table 1**
Treatment conditions.

| Sandblast grit | Sandblast pressure (MPa) | Sandblast distance (cm) | Sandblasti time (sec) | Acid treatment time (min) | Sample code |
|---|---|---|---|---|---|
| Alumina | — | — | — | — | NO |
| (50 μm) | — | — | — | 15 | NO-A |
| | 0.20 | 1 | 60 | — | — |
| | 0.20 | 5 | 60 | — | — |
| | 0.20 | 10 | 60 | — | — |
| | 0.20 | 20 | 60 | — | — |
| | 0.10 | 10 | 60 | — | — |
| | 0.15 | 10 | 60 | — | — |
| | 0.20 | 10 | 60 | — | — |
| | 0.25 | 10 | 60 | — | — |
| | 0.30 | 10 | 60 | — | — |
| | 0.20 | 10 | 30 | — | SB30 |
| | 0.20 | 10 | 30 | 15 | SB30-A |
| | 0.20 | 10 | 60 | — | SB60 |
| | 0.20 | 10 | 60 | 15 | SB60-A |
| | 0.20 | 10 | 90 | — | SB90 |
| | 0.20 | 10 | 90 | 15 | SB90-A |
| | 0.20 | 10 | 120 | — | SB120 |
| | 0.20 | 10 | 120 | 15 | SB120-A |

NO = No sandblast
NO-A = No sandblast; acid treatment
SB30 = Sandblast for 30 s
SB30-A = Sandblast for 30 s; acid treatment
SB60 = Sandblast for 60 s
SB60-A = Sandblast for 60 s; acid treatment
SB90 = Sandblast for 90 s
SB90-A = Sandblast for 90 s; acid treatment
SB120 = Sandblast for 120 s
SB120-A = Sandblast for 120 s; acid treatment.

adhesive strength by using polymers (such as hydrophobically-modified gelatin [21], dissipative hydrogels coupled with bridging polymers [22], mussel-inspired adhesives containing dihydroxyphenyl groups [23] and gecko-inspired solid-state adhesives [24]) and ceramics (such as silica [25], hydroxyapatite [26] and octacalcium phosphate [27]). However, polymers have limitations related to their mechanical strength and ceramics show a brittle property.

We recently reported that grade 1 commercially-pure Ti (CpTi) [28] and grade 5 Ti-6Al-4V alloy [29] films (thickness, 15–50 μm), after acid treatment with a $H_2SO_4$/HCl solution and air drying, showed a remarkable soft tissue adhesiveness immediately (*i.e.*, within a few seconds) after attachment onto soft tissues, as demonstrated by *ex vivo* shear adhesion tests with mouse dermal tissues. Of note, the acid treatment for implantable devices and currently-used electrical stimulation therapy devices whose outer casings are usually made of Ti would be applicable for easy and effective immobilization of the devices in connective tissues. Besides, the application of acid treatment in the neck area of Ti dental implant abutments in contact with non-keratinized soft tissues might be useful for the early formation and long-standing maintenance of peri-implant structures with effective biological barrier for protection against pathogen infiltration. For these future applications, the enhancement of immediate soft tissue adhesiveness would be important.

The adhesion strength depends generally on the interaction between adhesives and adherends as well as the interfacial area between them. Sandblasting is the operation of forcibly propelling a stream of abrasive material against a surface under high pressure to roughen a smooth surface [30]. The sandblasting pretreatment followed by acid etching is now used for Ti dental implants for enhancing osseointegration (*i.e.*, bonding to hard tissues through increasing the interlocking capacity of the surface) [31,32], which takes several months due to the complex processes including protein adsorption, cell adhesion and cell differentiation followed by bone remodeling [30]. However, the influence of sandblasting on the immediate soft-tissue adhesion of Ti is still unknown.

Herein, we evaluated the effects of sandblasting pretreatment conditions for CpTi in terms of the sandblasted surface area and the degree of deformation (*i.e.*, internal stress formation) of films. The effect of the sandblasting pretreatment on the immediate soft tissue adhesion of acid-treated CpTi was also investigated by using an *ex vivo* shear adhesion test with mouse dermal tissues. Finally, the sandblasting-optimized acid-treated CpTi adhesive was applied for immobilizing NFC devices *in vivo*.

## 2. Experimental

### 2.1. Materials

Cold-rolled thin CpTi (grade 1) films of 15 μm in thickness (TR2700C-H; Takeuchi Kinzokuhakuhun Kogyo Co. Ltd., Tokyo, Japan) were used to observe the film deformation, which reflects the internal stress formation and fatigue resistance, by sandblasting [33]. The film was cut into strips (5 mm × 35 mm), washed sequentially with acetone and pure water, and dried in the air before use. Unless otherwise stated, all materials were guaranteed reagent-grade and used as received from FUJIFILM Wako Pure Chemical Corporation (Osaka, Japan). Milli-Q water (Millipore Corp., Bedford, MA, USA) with a specific resistance of $18.2 \times 10^6$ Ω·cm was used.

### 2.2. Sandblasting and acid treatment

The CpTi films were fixed at both ends (around 2 mm) on a slide glass with a tape, and sandblasted (upper side only) with 50 μm alumina ($Al_2O_3$) particles using a laboratory sandblaster (Hi-Blaster III, Shofu Inc., Kyoto, Japan) at different conditions listed in Table 1. After sandblasting, both edges were cut, and each film (5 mm × 30 mm) was separately cleaned three times with pure water in an ultrasonic cleaner (ASU-2D; AS ONE Corp., Osaka, Japan) set at 23 kHz for 1 min. The washed film was then dried in the air at room temperature.

The dried films were immersed in an immediately-mixed solution of 97 wt% $H_2SO_4$ and 35 wt% HCl in water (final composition: 45 wt% $H_2SO_4$ and 15 wt% HCl) in a glass tube, which was subsequently soaked in a water bath at 70 °C. After 15 min, the acid solution was aspirated, and the films were washed thoroughly with water until complete pH neutralization. The washed films were dried in the air at 60 °C for 24 h.

### 2.3. Basic characterizations

The surface morphology of the film was observed with a 5 kV scanning electron microscope (SEM: JSM-6701 F; JEOL Ltd., Tokyo, Japan) available at the Central Research Laboratory in Okayama University Medical School after the samples were dried onto an aluminum stub and coated with osmium (Neoc-Pro, Meiwafosis Co. Ltd., Tokyo, Japan). The sandblasted surface area (%) was calculated by using an image analysis program (Image J; National Institutes of Health, Bethesda, MD, USA) for each SEM image taken at × 250 magnification ($N = 5$). The cross-section of the film was observed with a reflection microscope (MM-11; Nikon Nikon Solutions Co. Ltd., Tokyo, Japan) after the film was embedded in epoxy resin (EpoFix Resin; Struers, Copenhagen, Denmark) followed by grinding and polishing with #3000 silicon carbide abrasive papers (Buehler, a division of Illinois Tool Works Inc., Lake Bluff, IL, USA).

The calculated average surface roughness (*Ra*) of each sample was determined using a profilometer (HandySurf E-35B; Mitutoyo Corp., Kanagawa, Japan) with an active tip radius of 2 μm, reading length of 1.0 mm, and reading speed of 0.6 mm/s. Ten measurements at different locations, with the distance between each parallel track set to at least 0.5 mm, were recorded for each sample group.

Crystallographic analysis was conducted by X-ray diffraction (XRD) measurements (RINT2500HF; Rigaku Corp., Tokyo, Japan) using Cu-Kα

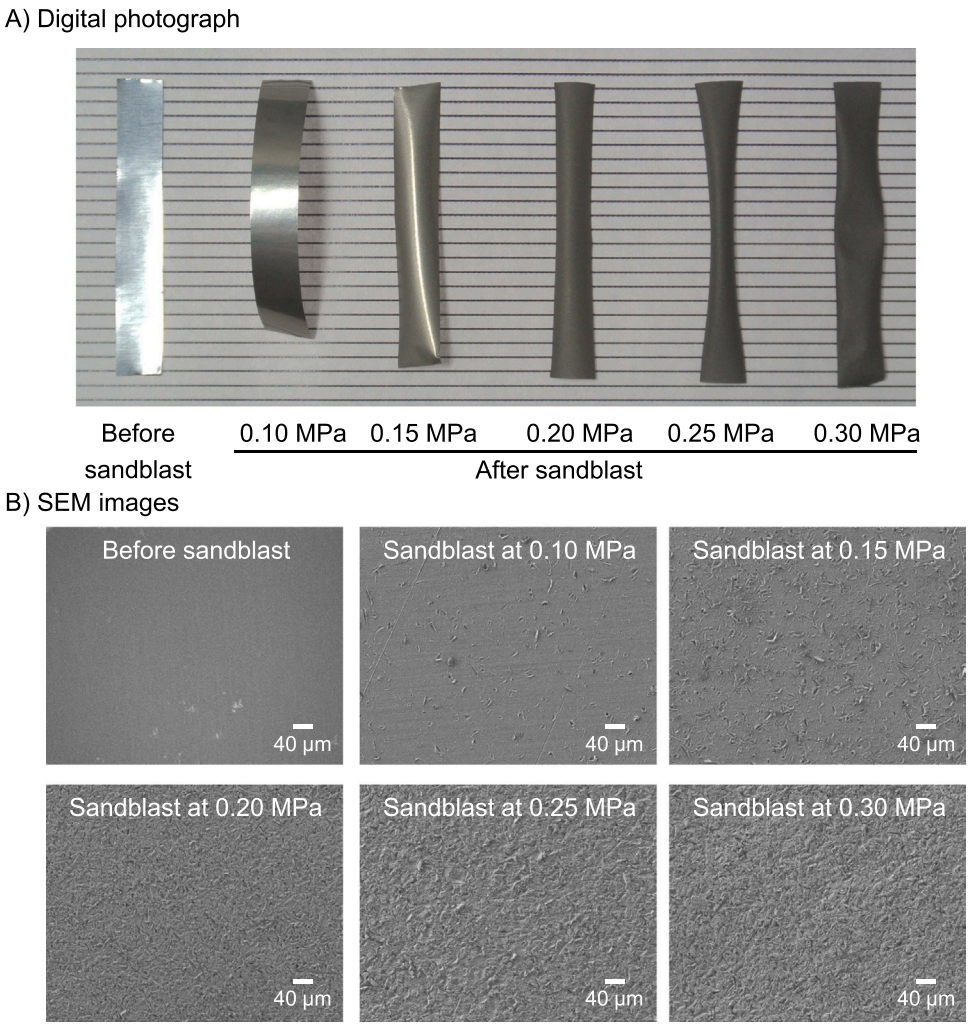


**Fig. 1.** (A) Digital photograph and (B) SEM images of CpTi films after sandblasting (10 cm; 60 s) at different pressure conditions. The sandblasted surfaces were set upward.

(1.54 Å) irradiation at 40 kV and 200 mA. The XRD measurements were conducted from 20° to 65° at a scan speed of 2°/min. Each peak area of the XRD pattern was calculated by an XRD pattern analysis program (JADE 5.0; Materials Data, Inc., Livermore, CA, USA).

Static water contact angles (WCA) in the air were measured after the droplets (10 μL) were placed on the film surfaces. The static contact angle was calculated based on a half-angle method ($N = 5$).

### 2.4. Immediate soft-tissue adhesiveness

All the animal procedures undertaken in this study were strictly in accordance with the Guidelines for Animal Experiments at Okayama University after approval of the experimental protocol by Okayama University (OKU-2020530).

First, *ex vivo* shear adhesion tests were conducted for quantitative evaluation of the immediate soft tissue adhesion property, which would involve mainly chemical and/or physical interactions, but not cells, and be critical for initial immobilization of the device in living bodies. The shaved skin tissues were excised from the back of 6 week-old male BALB/c mice (Japan SLC, Inc., Shizuoka, Japan) after being euthanized with $CO_2$ gas or an overdose of isoflurane. The reticular dermal layer was exposed by removing the superficial fascia, trimmed into 5 mm × 40 mm strips, immersed in a saline solution (0.9 w/v% NaCl solution), and used within 6 h after isolation. After the excess amount of saline solution on the trimmed tissues was removed with filter papers, the CpTi film was attached to the tissue with an overlapping area of 5 mm × 2 mm, as reported previously [28]. Shear adhesion tests were performed with a mechanical tester (Ez-test; Shimadzu Corp., Kyoto, Japan) at a speed of 150 mm/min. The apparent shear adhesion strength was calculated from the maximum load (fracture force) divided by the overlapping area ($N = 5$). After the adhesion tests, the CpTi surfaces were observed with a reflection microscope (MM-11), and the remained organics stained with eosin were analyzed with an image analysis program (Image J) for each photograph ($N = 4$).

### 2.5. Implantation tests

The non-treated or sandblast/acid-treated CpTi film after autoclave sterilization was attached to the bottom side of an NFC light emission device (size: 7.0 mmW, 11.0 mmH, 0.8 mmT; KP-NFLER for red light emission or KP-NFLEG for green light emission; KYOHRITSU Electronic Industry Co. Ltd., Osaka, Japan) having a pressure-sensitive adhesive layer on the bottom. The devices attached with either the non-treated or sandblast/acid-treated CpTi films were respectively placed onto the fascia on the right and left sides of the dorsal region of a six-week-old male BALB/c mouse (Japan SLC, Inc.). The non-contact power supply was conducted by iPhoneX (Apple Inc., Cupertino, CA, USA) controlled with an iOS application (NFC Tools-iOS; WAKDEV). After the non-contact power supply test (around 10 min), the skin was incised again, and the device was peeled off with tweezers.

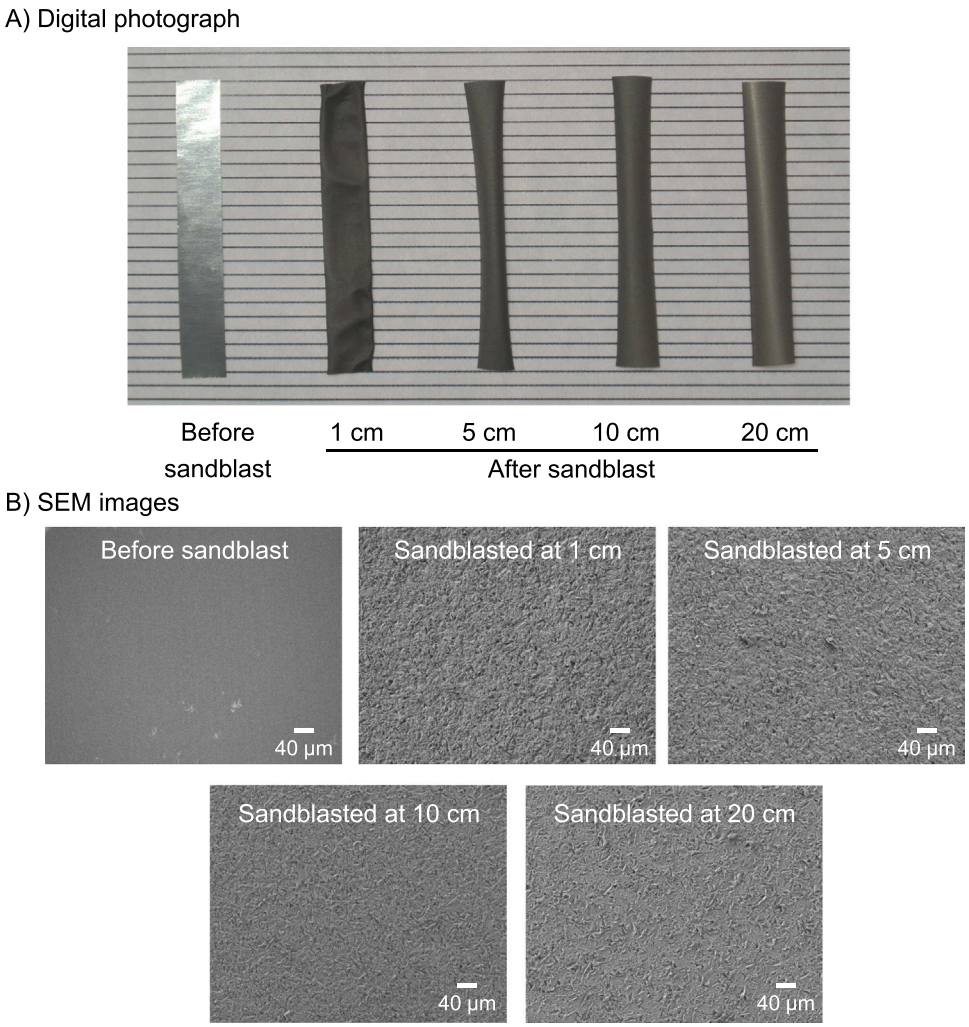


**Fig. 2.** (A) Digital photograph and (B) SEM images of CpTi films after sandblasting (0.2 MPa; 60 s) at different distances. The sandblasted surfaces were set upward.

### 2.6. Statistical analysis

After the normality and homogeneity of variance were tested using the Shapiro-Wilk and Bartlett tests, respectively, the Tukey-Kramer test was used for intergroup comparative analysis. All statistical tests were performed using R (version 3.3.2) [34] at preset alpha levels of 0.05.

## 3. Results and discussion

### 3.1. Sandblasting conditions

In order to explore the optimal sandblasting pretreatment conditions, the sandblasting pressure, distance and time were evaluated at varied conditions (Table 1). Alumina particles with irregular shapes were used as a sandblasting grit due to their excellent material properties, and the irregular shape can effectively prepare the primary roughness with micro-scale pits [35].

#### 3.1.1. Sandblasting pressure

First, the effect of sandblasting pressure was evaluated at a constant time (60 s) and distance (10 cm). After sandblasting, the macroscopic deformation and the sandblasted surface area (%), determined from SEM image analysis, of CpTi films were evaluated. In the case of the lowest sandblasting pressure at 0.10 MPa, the films were rolled largely after sandblasting (Fig. 1**A**), indicating the release of the internal stress formed during cold rolling process of the film and/or the surface expansion on the sandblasted side [33]. The degree of curling in the films was the lowest after sandblasting at 0.15 MPa; however, the intact surface was observed (sandblasted surface area, 29 ± 3%) even after the long-term sandblasting (60 s) from SEM observation (Fig. 1**B**). The entire surface was sandblasted at conditions above 0.20 MPa (sandblasted surface area, 100%); however, the films were further curled (at 0.25 MPa) or wrinkled (at 0.30 MPa) at higher pressure (Fig. 1**A**). From these results, the optimal sandblasting pressure was set to 0.20 MPa in this study.

#### 3.1.2. Sandblasting distance

The effect of sandblasting distance was evaluated at a constant time (60 s) and pressure (0.2 MPa). The CpTi film sandblasted at 1 cm was wrinkled, which would be due to locally generated large stress at the short sandblasting distance. However, sandblasting at 5 cm or more did not induce film wrinkling. (Fig. 2**A**). The degree of curling tended to decrease by increasing the sandblasting distance, and the sandblasted surface area was 100% in all conditions, except in the case of the sandblasting at 20 cm (sandblasted surface area, 93 ± 2%), as shown by the SEM images (Fig. 2**B**). From these results, the optimal sandblasting distance was set to 10 cm in this study.

#### 3.1.3. Sandblasting time

The effect of sandblasting time was evaluated at constant pressure (0.2 MPa) and distance (10 cm). The degree of film curling tended to increase by increasing the sandblasting time, and the film was wrinkled

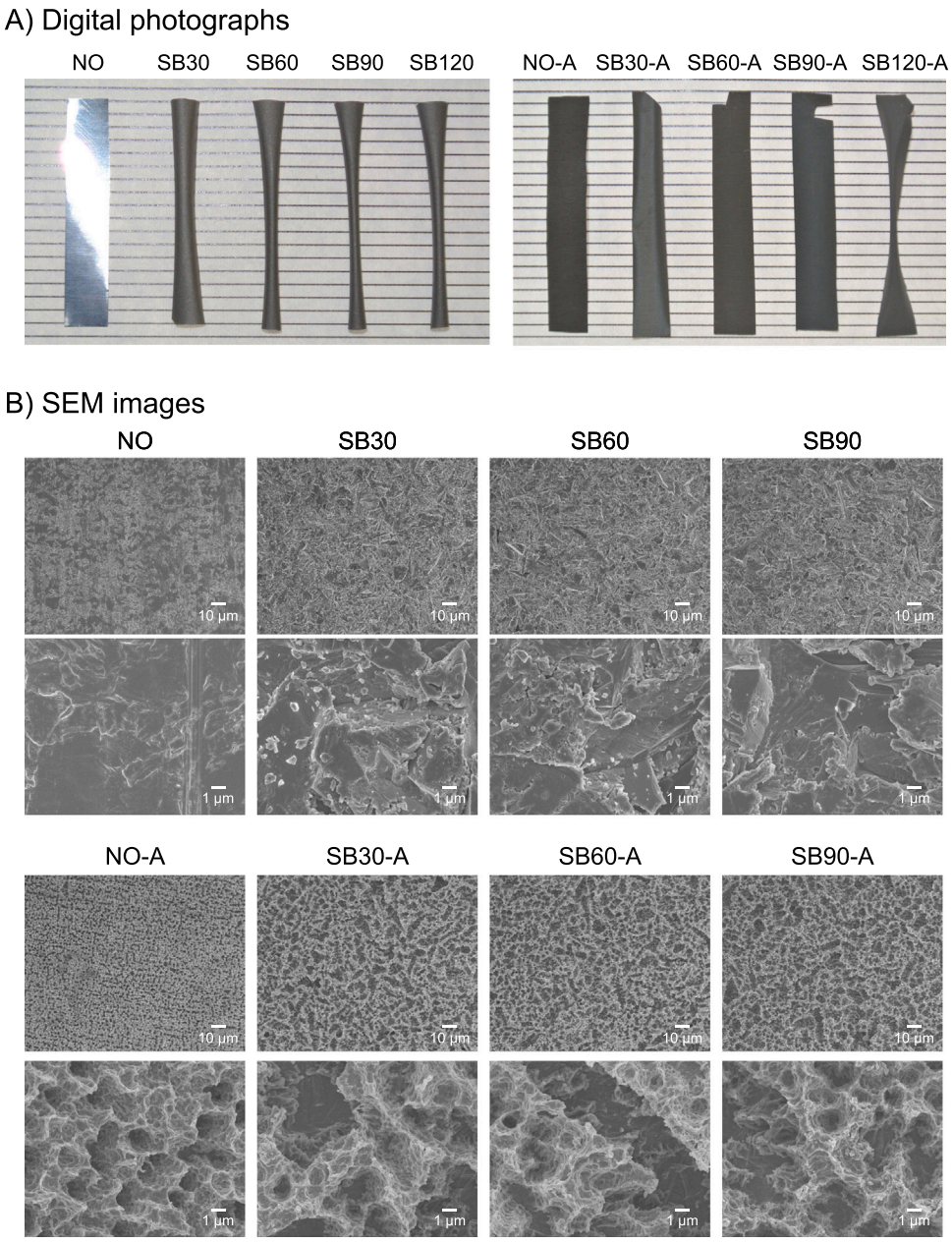


**Fig. 3.** (A) Digital photograph and (B) SEM images of CpTi films after sandblasting (0.2 MPa; 10 cm) at different times followed by acid treatment. The sandblasted surfaces were set upward. The sample codes are shown in Table 1.

after sandblasting for 120 s (Fig. 3**A**). The intact surface was observed only in the case of sandblasting for 30 s (sandblasted surface area, 89 ± 4%), as from the SEM observations (Fig. 3**B**). The film thickness tended to decrease slightly by increasing the sandblasting time (Fig. 4**A**). There was no significant difference in the surface roughness (*Ra*) of CpTi films after sandblasting at different time periods (Fig. 4**B**). In this study, the CpTi films sandblasted at different time periods (0–90 s) were acid treated and their soft-tissue adhesion strengths were compared in order to eliminate the influence of large rolling or wrinkling of CpTi films.

### 3.2. Acid treatment after sandblasting

The acid treatments were conducted with a mixed acid solution (45 wt% $H_2SO_4$ and 15 wt% HCl) in a glass tube at 70 °C. In the case of the samples without sandblasting, bubbles were formed after approximately 9-min acid treatment and the solution color gradually turned into purple, indicating the dissolution of metallic Ti and the formation of $H_2$ gas [36] after removal of the oxidized surface layer. On the other hand, in the case of the samples after sandblasting, the bubbles were formed earlier (at approximately 5 min). Besides, the films without sandblasting were dissolved macroscopically at around 25 min, whereas the sandblasted counterparts were dissolved at around 20 min (data omitted). These results suggest that the thick oxidized layer, which must be formed during cold roll processing of thin film, was removed by sandblasting [37]. Of note, the increased surface area and surface activity of sandblasted Ti surfaces would be another factor reducing the accelerated etching reaction [38,39]. Therefore, the acid treatment time was set to 15 min in this study.

After acid treatment, the deformation of the film by sandblasting was recovered (Fig. 3**A**), indicating the removal of the expanded surface layer by dissolution. SEM observation revealed nano-sized structures on the film surfaces after acid treatment (Fig. 3**B**). From the cross-sectional observation (Fig. 4**A**), the sandblasted film became thinner after the acid treatment compared with the non-sandblasted counterparts, which

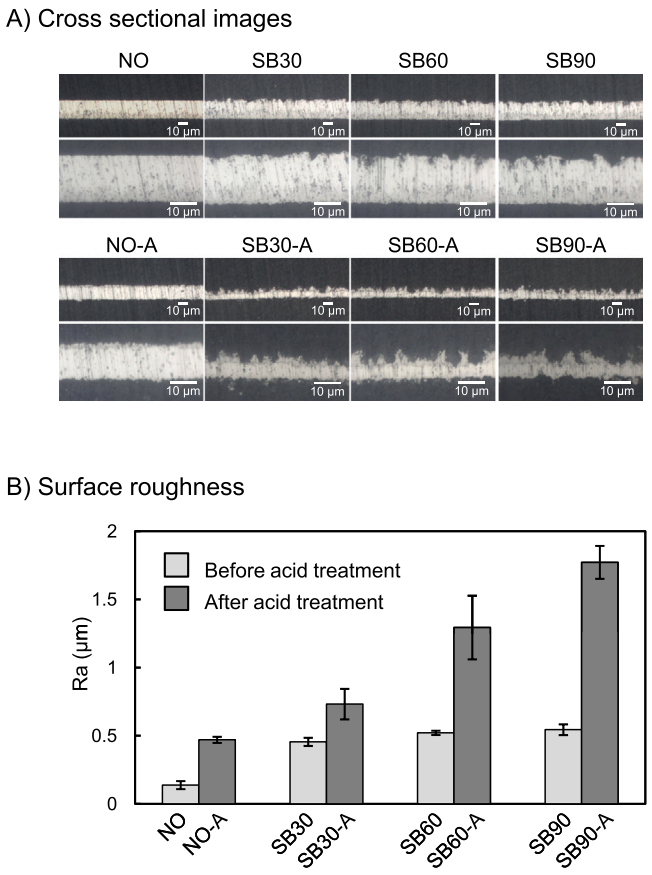


**Fig. 4.** (A) Optical micrographs of ground cross sections and (B) surface roughness (*Ra*) of CpTi films after sandblasting (0.2 MPa; 10 cm) at different times followed by acid treatment. The sample codes are shown in Table 1.

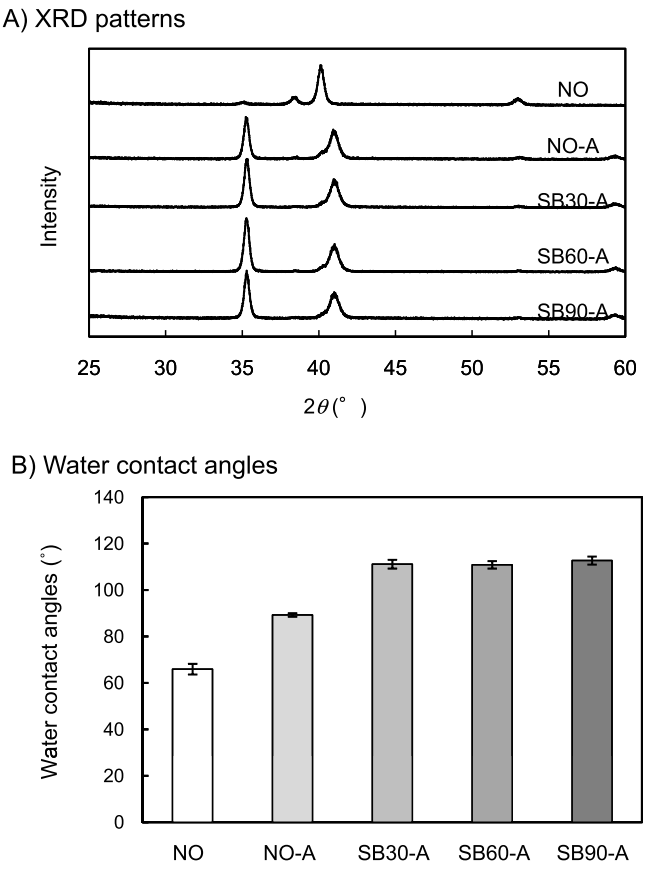


**Fig. 5.** (A) XRD patterns and (B) water contact angles of CpTi films after sandblasting (0.2 MPa; 10 cm) at different times followed by acid treatment. The sample codes are shown in Table 1.

would be due to the removal of the oxidized surface layers by acid etching and the increased surface area after sandblasting. Of note, thinning of the material causes a reduction of mechanical properties, and hence the initial thickness of CpTi should be optimized when considering its final application. The *Ra* values of the acid-treated films increased linearly by increasing sandblasting times (Fig. 4**B**).

Crystallographic analysis (Fig. 5**A**) revealed that the surfaces of the CpTi films consisted of α-Ti and δ-$TiH_x$, which could be formed by the reaction between Ti and $H_2$ generated by the oxidation reaction of Ti during acid treatment [36,40,41] without the formation of any crystalline $TiO_2$ after acid treatment. Of note, there is no clear difference in the XRD patterns of the sandblasted and non-sandblasted films after acid treatment. The acid-treated CpTi films showed a hydrophobic surface (WCA, around 90°), as reported in a previous study [41], and the WCAs were increased to around 110° by sandblast pretreatment (Fig. 5**B**). The increased WCA would be due to the increased *Ra* value (Fig. 4**B**); however, there was no significant difference in WCAs among the sandblasted samples.

### 3.3. Immediate soft-tissue adhesion strength

The acid-treated CpTi adhered immediately (*i.e.*, within a few seconds) to a hydrous soft tissue by gentle pressure. For quantitative analysis of soft tissue adhesiveness, the CpTi films were attached to mouse reticular dermal tissue (contact area, 5 ×2 $mm^2$) and *ex vivo* shear adhesion tests were conducted. The reticular dermal tissue is the central and largest layer of the dermis, consisting of thick and highly organized collagen fiber bundles with low cellular density [42], and hence the *ex vivo* test in this study would reflect the immediate adhesion of CpTi to soft tissues, which is mainly based on chemical and/or physical interactions, but not cells, and strongly supports the initial immobilization of implant devices.

While the sandblasted CpTi films without acid treatment showed almost no adhesion to the mouse dermal tissue (data omitted), the acid-treated CpTi films showed substantial soft tissue adhesion (Fig. 6**A**). In the previous study [28], it was estimated that the immediate adhesion of acid-treated CpTi was caused by hydrophobic interactions with hydrophobic components of extracellular matrix (ECM), as demonstrated by the characteristics of the acid-treated CpTi surface and the ECM components remained attaching on the CpTi surfaces after the adhesion test. Of note, hydrophobic surfaces generally show larger protein adsorption amount and faster protein adsorption rate compared with hydrophilic surfaces [43]. Besides, hydrophobic surfaces show stronger adhesion force with several kinds of proteins compared with hydrophilic surfaces [44].

The *ex vivo* immediate soft tissue adhesion strength of acid-treated CpTi increased significantly by sandblast pretreatments (Fig. 6**A**), reaching the highest value after sandblasting for 60 s. The highest adhesion strength (102 ± 19 kPa) of the sandblast/acid-treated CpTi was significantly higher than that of a commercially available fibrin glue (*e.g.,* 18 kPa [26]) or GRFG glue (*e.g.*, 48 kPa at wet conditions [23]). After the adhesion tests, fibrous tissues (*i.e.*, collagen fiber bundles and split collagen fibers) remained attaching on the sandblast/acid-treated CpTi films (Fig. 6**B and C**), indicating the cohesive failure of fibrous dermal tissues. Of note, there was no significant difference in the adhesion strengths between the films sandblasted for 60 and 90 s, which might suggest that the soft tissues could not infiltrate into deep pores on the CpTi surface under the contact conditions used in this study.

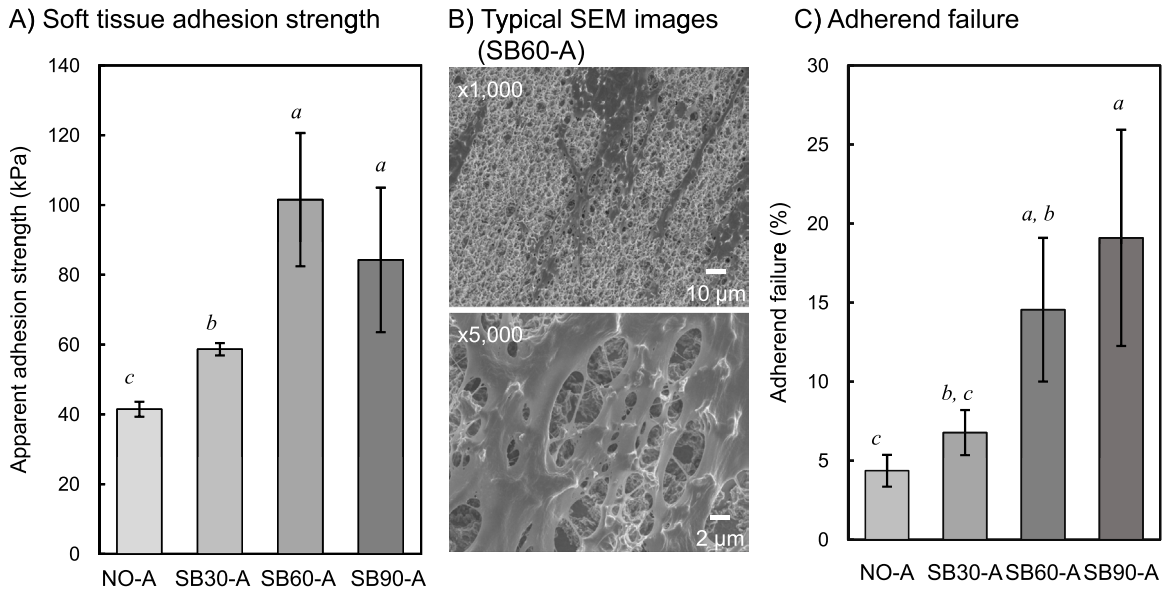


**Fig. 6.** (A) Apparent adhesion strength of CpTi films to mouse dermal tissues ($N = 5$). The different italic letters (*a* and *b*) on bars indicate statistically significant differences between the groups in each graph, as determined by Tukey–Kramer test ($p < 0.05$). (B) SEM images of SB60-A surface after the adhesion test. (C) Adherend failure rates determined after the adhesion test.

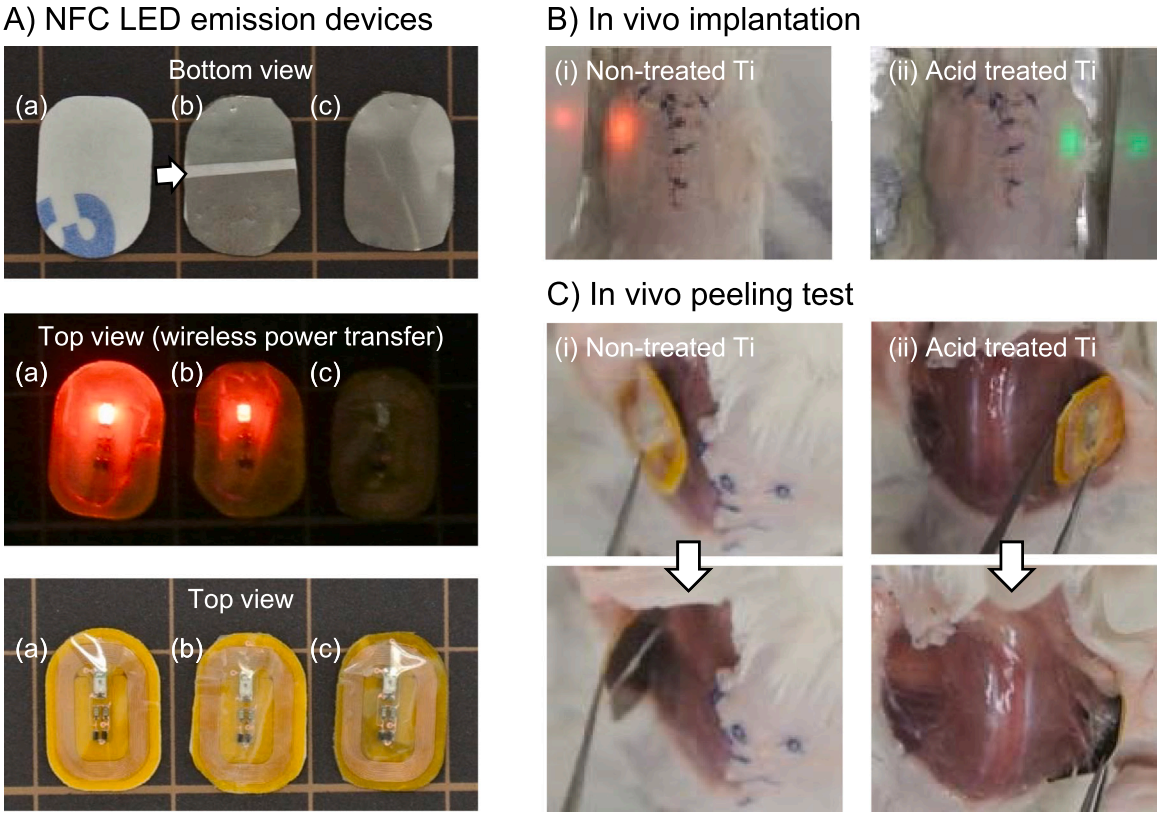


**Fig. 7.** Self-adhering implantable devices. (A) LED NFC emission devices: (a) without CpTi; (b) with two CpTi films attached separated by a 1 mm gap (arrow); (c) with one CpTi film covering the entire bottom surface of the device. (B) The wireless power transfer to the NFC devices implanted subcutaneously in a back of a mouse. (C) The NFC devices were peeled after the implantation. In the photographs (B) and (C), the device with the (i) non-treated and (ii) acid-treated CpTi films with a 1 mm gap were implanted on the left and right sides, respectively. The NFC device with non-treated CpTi film could be easily detached from the fascia, while that with acid-treated CpTi film was strongly adhered to the fascia (see also Supplemental Movie S2).

### *3.4. In vivo immobilization of an implantable device by Ti adhesive*

A significant application of self-adhering Ti films (or direct acid treatment of Ti device surfaces) is for an easy and effective immobilization of body-implanted biochips and biosensors to obtain more precise and accurate real-time information from the inner tissues or organs. In order to demonstrate the application of sandblast/acid-treated CpTi adhesives for immobilization of devices without suturing

nor organic glues *in vivo*, an NFC light emission device (7.0 mmW × 11.0 mmH × 0.8 mmT) attached with the CpTi adhesive films was placed on the muscle fascia in the dorsal region of a mouse. Of note, the non-contact power supply was blocked when the entire NFC antenna was covered with CpTi film; however, the light emission was observed by placing two CpTi films separately with a gap (Fig. 7**A**). At the gap distance of 1 mm, the light emission intensity was around 50% compared to that of the device without CpTi. The NFC devices also worked after implantation *in vivo* (Fig. 7**B**; see also Supplemental Movie S1), although the device attached with the non-treated CpTi easily moved (Fig. 7**C**; see also Supplemental Movie S2A). The direct and strong adhesion of the acid-treated CpTi to the fascia tissue could be demonstrated by compulsory removal (Fig. 7**C**; see also Supplemental Movie S2B).

After initial immobilization, it is also expected that the implanted devices would be encapsulated with and immobilized more strongly to connective tissues during physiological healing process, because acid-treated rough CpTi (grade 2) dental implants in subcutaneous tissues were encapsulated more stably as compared with polished Ti [45]. However, the interface formed between Ti and non-keratinized soft tissues has been much less studied [46] and material surface characteristics including submicron- and nano-scale roughness are recognized as important factors in implant-related infections [47]. Therefore, further biological evaluations (*e.g.*, mechanical, chemical and biological safety including bacterial infections and degree of device migration) for application as a new self-adhering implant device in soft tissues should be necessary in the future.

## 4. Conclusions

The optimum sandblasting pretreatment enhanced the soft tissue adhesiveness of acid-treated CpTi remarkably. This strategy would be an effective method for the development of self-adhering implantable devices, which can be immobilized inside the bodies without suturing nor organic glues.

## CRediT authorship contribution statement

**Atsushi Yabe**: Investigation, Formal analysis, Visualization Writing – original draft. **Masahiro Okada**: Conceptualization, Methodology, Validation, Writing – review & editing, Project administration, Funding acquisition. **Emilio Satoshi Hara**: Investigation, Writing – review & editing. **Yasuhiro Torii**: Supervision. **Takuya Matsumoto**: Conceptualization, Writing – review & editing, Funding acquisition.

## Declaration of Competing Interest

The authors declare that they have no known competing financial interests or personal relationships that could have appeared to influence the work reported in this paper.

## Acknowledgements

This work was supported partly by the Japan Society for the Promotion of Science (JSPS KAKENHI grant numbers: JP20H05225, JP21K12683, JP21K18828 and JP21H03123), Japan.

## Appendix A. Supporting information

Supplementary data associated with this article can be found in the online version at doi:10.1016/j.colsurfb.2021.112283.

## References

[1] C. Smith, Human microchip implantation, J. Technol. Manag. Innov. 3 (2008) 151–160, https://doi.org/10.4067/S0718-27242008000100015.
[2] H.C. Koydemir, A. Ozcan, Wearable and implantable sensors for biomedical applications, Annu. Rev. Anal. Chem. 11 (2018) 127–146, https://doi.org/10.1146/annurev-anchem-061417-125956.
[3] M. Gray, J. Meehan, C. Ward, S.P. Langdon, I.H. Kunkler, A. Murray, D. Argyle, Implantable biosensors and their contribution to the future of precision medicine, Vet. J. 239 (2018) 21–29, https://doi.org/10.1016/j.tvjl.2018.07.011.
[4] P.R. Troyk, Injectable electronic identification, monitoring, and stimulation systems, Annu. Rev. Biomed. Eng. 1 (1999) 177–209, https://doi.org/10.1146/annurev.bioeng.1.1.177.
[5] K. Scholten, E. Meng, A review of implantable biosensors for closed-loop glucose control and other drug delivery applications, Int. J. Pharm. 544 (2018) 319–334, https://doi.org/10.1016/j.ijpharm.2018.02.022.
[6] ISO 15639-1, Radio frequency identification of animals – Standardization of injection sites for different animal species – Part 1: Companion animals (cats and dogs), 2015.
[7] T.M. Norton, K.M. Andrews, L.L. Smith, Techniques for working with wild reptiles, in: D.R. Mader, S.J. Divers (Eds.), Current Therapy in Reptile Medicine and Surgery, Elsevier, St. Louis, Missouri, 2014, pp. 310–340, https://doi.org/10.1016/B978-1-4557-0893-2.00029-6.
[8] M.T. Bennett, S.K.K. Tung, Long-term efficacy of cardiac pacemakers and implantable cardioverter/defibrillators, J. Long Term Eff. Med. Implants 20 (2010) 187–202, https://doi.org/10.1615/jlongtermeffmedimplants.v20.i3.30.
[9] T. Morishita, J.D. Hilliard, M.S. Okun, D. Neal, K.A. Nestor, D. Peace, A.A. Hozouri, M.R. Davidson, F.J. Bova, J.M. Sporrer, G. Oyama, K.D. Foote, Postoperative lead migration in deep brain stimulation surgery: incidence, risk factors, and clinical impact, PLoS One 12 (2017), e0183711, https://doi.org/10.1371/journal.pone.0183711.
[10] S. Eldabe, E. Buchser, R.V. Duarte, Complications of spinal cord stimulation and peripheral nerve stimulation techniques: a review of the literature, Pain Med. 17 (2016) 325–336, https://doi.org/10.1093/pm/pnv025.
[11] R.G. Bowman, D. Caraway, I. Bentley, Comparison of a novel fixation device with standard suturing methods for spinal cord stimulators, Neuromodulation 16 (2013) 454–458, https://doi.org/10.1111/j.1525-1403.2012.00480.x.
[12] S. Koulouris, S. Pastromas, A.S. Manolis, An unusual distal abdominal migration of a pacemaker pulse generator with a complete epicardial lead fracture, EP Europace 10 (2008) 1461, https://doi.org/10.1093/europace/eun281.
[13] J.L. Ward, T.C. Defrancesco, S.P. Tou, C.E. Atkins, E.H. Griffith, B.W. Keene, Complication rates associated with transvenous pacemaker implantation in dogs with high-grade atrioventricular block performed during versus after normal business hours, J. Vet. Intern. Med. 29 (2015) 157–163, https://doi.org/10.1111/jvim.12512.
[14] I. Russi, R. Liechti, E. Memeti, S. Bertschy, V. Weberndoerfer, R. Kobza, Intracolonic cardiac pacemaker: a case of device migration with colon perforation out of a subcutaneous epifascial pocket, Hear. Case Rep. 4 (2018) 497–500, https://doi.org/10.1016/j.hrcr.2018.04.006.
[15] A. Lauto, D. Mawad, L.J.R. Foster, Adhesive biomaterials for tissue reconstruction, J. Chem. Technol. Biotechnol. 83 (2008) 464–472, https://doi.org/10.1002/jctb.1771.
[16] A. Dodge-Khatami, C.L. Backer, M. Meuli, R. Prêtre, M. Tomaske, C. Mavroudis, Migration and colon perforation of intraperitoneal cardiac pacemaker systems, Ann. Thorac. Surg. 83 (2007) 2230–2232, https://doi.org/10.1016/J.ATHORACSUR.2006.12.037.
[17] Y.-C. Tseng, H. Suong-Hyu, Y. Ikada, Y. Shimizu, K. Tamura, S. Hitomi, In vivo evaluation of 2-cyanoacrylates as surgical adhesives, J. Appl. Biomater. 1 (1990) 111–119, https://doi.org/10.1002/jab.770010203.
[18] S. Fukunaga, M. Karck, W. Harringer, J. Cremer, C. Rhein, A. Haverich, The use of gelatin-resorcin-formalin glue in acute aortic dissection type A, Eur. J. Cardio Thorac. Surg. 15 (1999) 564–570, https://doi.org/10.1016/S1010-7940(99)00084-6.
[19] E.V. Dare, M. Griffith, P. Poitras, T. Wang, G.F. Dervin, A. Giulivi, M.T. Hincke, Fibrin sealants from fresh or fresh/frozen plasma as scaffolds for in vitro articular cartilage regeneration, Tissue Eng. Part A 15 (2009) 2285–2297, https://doi.org/10.1089/ten.tea.2008.0228.
[20] M. Matsuda, M. Inoue, T. Taguchi, Adhesive properties and biocompatibility of tissue adhesives composed of various hydrophobically modified gelatins and disuccinimidyl tartrate, J. Bioact. Compat. Polym. 27 (2012) 481–498, https://doi.org/10.1177/0883911512455116.
[21] A. Nishiguchi, Y. Kurihara, T. Taguchi, Underwater-adhesive microparticle dressing composed of hydrophobically-modified Alaska pollock gelatin for gastrointestinal tract wound healing, Acta Biomater. 99 (2019) 387–396, https://doi.org/10.1016/J.ACTBIO.2019.08.040.
[22] J. Li, A.D. Celiz, J. Yang, Q. Yang, I. Wamala, W. Whyte, B.R. Seo, N.V. Vasilyev, J. J. Vlassak, Z. Suo, D.J. Mooney, Tough adhesives for diverse wet surfaces, Science 357 (2017) 378–381, https://doi.org/10.1126/science.aah6362.
[23] V. Bhagat, M.L. Becker, Degradable adhesives for surgery and tissue engineering, Biomacromolecules 18 (2017) 3009–3039, https://doi.org/10.1021/acs.biomac.7b00969.
[24] A. Mahdavi, L. Ferreira, C. Sundback, J.W. Nichol, E.P. Chan, D.J.D. Carter, C. J. Bettinger, S. Patanavanich, L. Chignozha, E. Ben-Joseph, A. Galakatos, H. Pryor, I. Pomerantseva, P.T. Masiakos, W. Faquin, A. Zumbuehl, S. Hong, J. Borenstein, J. Vacanti, R. Langer, J.M. Karp, A biodegradable and biocompatible gecko-inspired tissue adhesive, Proc. Natl. Acad. Sci. USA 105 (2008) 2307–2312, https://doi.org/10.1073/pnas.0712117105.
[25] S. Rose, A. Prevoteau, P. Elzière, D. Hourdet, A. Marcellan, L. Leibler, Nanoparticle solutions as adhesives for gels and biological tissues, Nature 505 (2014) 382–385, https://doi.org/10.1038/nature12806.

[26] M. Okada, A. Nakai, E.S. Hara, T. Taguchi, T. Nakano, T. Matsumoto, Biocompatible nanostructured solid adhesives for biological soft tissues, Acta Biomater. 57 (2017) 404–413, https://doi.org/10.1016/j.actbio.2017.05.014.
[27] Y. Sugiura, M. Okada, K. Hirano, T. Matsumoto, Bone mineral analogue ceramic block as an instant adhesive to biological soft tissue, Adv. Mater. Interfaces 8 (2021), 2002032, https://doi.org/10.1002/admi.202002032.
[28] M. Okada, E.S. Hara, A. Yabe, K. Okada, Y. Shibata, Y. Torii, T. Nakano, T. Matsumoto, Titanium as an instant adhesive for biological soft tissue, Adv. Mater. Interfaces 7 (2020), 1902089, https://doi.org/10.1002/admi.201902089.
[29] Y. Wang, M. Okada, S.C. Xie, Y.Y. Jiao, E.S. Hara, H. Yanagimoto, T. Fukumoto, T. Matsumoto, Immediate soft-tissue adhesion and mechanical properties of Ti-6Al-4V alloy after long-term acid treatment, J. Mater. Chem. B 9 (2021) 8348–8354, https://doi.org/10.1039/D1TB00919B.
[30] D.D. Bosshardt, V. Chappuis, D. Buser, Osseointegration of titanium, titanium alloy and zirconia dental implants: current knowledge and open questions, Periodontology 73 (2017) 22–40, https://doi.org/10.1111/prd.12179.
[31] F. Butz, T. Ogawa, I. Nishimura, Interfacial shear strength of endosseous implants, Int. J. Oral Maxillofac. Implants 26 (2011) 746–751. ⟨http://www.ncbi.nlm.nih.gov/pubmed/21841983⟩.
[32] S. Spriano, S. Yamaguchi, F. Baino, S. Ferraris, A critical review of multifunctional titanium surfaces: new frontiers for improving osseointegration and host response, avoiding bacteria contamination, Acta Biomater. 79 (2018) 1–22, https://doi.org/10.1016/J.ACTBIO.2018.08.013.
[33] F. Javier Gil, J.A. Planell, A. Padrós, C. Aparicio, The effect of shot blasting and heat treatment on the fatigue behavior of titanium for dental implant applications, Dent. Mater. 23 (2007) 486–491, https://doi.org/10.1016/j.dental.2006.03.003.
[34] R Development Core Team, R: A Language and Environment for Statistical Computing, 2016. ⟨http://www.r-project.org/⟩.
[35] S. Li, J. Ni, X. Liu, H. Lu, S. Yin, M. Rong, Z. Guo, L. Zhou, Surface characteristic of pure titanium sandblasted with irregular zirconia particles and Acid-Etched, Mater. Trans. 53 (2012) 913–919, https://doi.org/10.2320/matertrans.M2011291.
[36] N. Ren, G. Wang, H. Liu, T. Ohachi, In situ synthesis of $TiH_2$ layer on metallic titanium foil through gaseous hydrogen free acid-hydrothermal method, Mater. Res. Bull. 50 (2014) 379–384, https://doi.org/10.1016/J.MATERRESBULL.2013.11.002.
[37] M. Mizuhata, S. Yamamoto, H. Maki, Removal of surface scale from titanium metal by etching with HF-$HNO_3$ mixed acid, Mater. Trans. 58 (2017) 1280–1289, https://doi.org/10.2320/matertrans.M2017110.
[38] B.I. Johansson, B. Bergman, Corrosion of titanium and amalgam couples: effect of fluoride, area size, surface preparation and fabrication procedures, Dent. Mater. 11 (1995) 41–46, https://doi.org/10.1016/0109-5641(95)80007-7.
[39] E.S. Ogawa, A.O. Matos, T. Beline, I.S.V. Marques, C. Sukotjo, M.T. Mathew, E. C. Rangel, N.C. Cruz, M.F. Mesquita, R.X. Consani, V.A.R. Barão, Surface-treated commercially pure titanium for biomedical applications: electrochemical, structural, mechanical and chemical characterizations, Mater. Sci. Eng. C 65 (2016) 251–261, https://doi.org/10.1016/j.msec.2016.04.036.
[40] E. Conforto, D. Caillard, B.O. Aronsson, P. Descouts, Electron microscopy on Titanium implants for bone replacement after "SLA" surface treatment, Eur. Cells Mater. 3 (Suppl 1) (2002) 9–10.
[41] S. Ban, Y. Iwaya, H. Kono, H. Sato, Surface modification of titanium by etching in concentrated sulfuric acid, Dent. Mater. 22 (2006) 1115–1120, https://doi.org/10.1016/j.dental.2005.09.007.
[42] E. Rognoni, F.M. Watt, Skin cell heterogeneity in development, wound healing, and cancer, Trends Cell Biol. 28 (2018) 709–722, https://doi.org/10.1016/j.tcb.2018.05.002.
[43] G.B. Sigal, M. Mrksich, G.M. Whitesides, Effect of surface wettability on the adhesion of proteins and detergents, J. Am. Chem. Soc. 120 (1998) 3464–3473, https://doi.org/10.1021/ja970819l.
[44] A. Sethuraman, M. Han, R.S. Kane, G. Belfort, Effect of surface wettability on the adhesion of proteins, Langmuir 20 (2004) 7779–7788, https://doi.org/10.1021/la049454q.
[45] H. Kim, H. Murakami, B. Chehroudi, M. Textor, D.M. Brunette, Effects of surface topography on the connective tissue attachment to subcutaneous implants, Int. J. Oral Maxillofac. Implants 21 (2006) 354–365. ⟨http://www.ncbi.nlm.nih.gov/pubmed/16796277⟩.
[46] B.G.R. Zigterman, C. Van den Borre, A. Braem, M.Y. Mommaerts, Titanium surface modifications and their soft-tissue interface on nonkeratinized soft tissues—a systematic review (Review), Biointerphases 14 (2019), 040802, https://doi.org/10.1116/1.5113607.
[47] M. Wang, T. Tang, Surface treatment strategies to combat implant-related infection from the beginning, J. Orthop. Transl. 17 (2019) 42–54, https://doi.org/10.1016/j.jot.2018.09.001.